

SUPERVISED LEARNING FROM NOISY OBSERVATIONS: COMBINING MACHINE-LEARNING TECHNIQUES WITH DATA ASSIMILATION

GEORG A. GOTTWALD

*School of Mathematics and Statistics
University of Sydney
NSW 2006
Australia*

SEBASTIAN REICH

*Institute of Mathematics
University of Potsdam
Germany*

ABSTRACT. Data-driven prediction and physics-agnostic machine-learning methods have attracted increased interest in recent years achieving forecast horizons going well beyond those to be expected for chaotic dynamical systems. In a separate strand of research data-assimilation has been successfully used to optimally combine forecast models and their inherent uncertainty with incoming noisy observations. The key idea in our work here is to achieve increased forecast capabilities by judiciously combining machine-learning algorithms and data assimilation. We combine the physics-agnostic data-driven approach of random feature maps as a forecast model within an ensemble Kalman filter data assimilation procedure. The machine-learning model is learned sequentially by incorporating incoming noisy observations. We show that the obtained forecast model has remarkably good forecast skill while being computationally cheap once trained. Going beyond the task of forecasting, we show that our method can be used to generate reliable ensembles for probabilistic forecasting as well as to learn effective model closure in multi-scale systems.

1. INTRODUCTION

Data-driven physics-agnostic modelling has attracted a great deal of interest in recent years. Such models have become particularly attractive for modelling high-dimensional complex systems where the detailed evolutionary laws are either unknown

E-mail addresses: georg.gottwald@sydney.edu.au, sebastian.reich@uni-potsdam.de.

or are too complex to be resolved numerically, and provide a desirable cost-effective alternative to the numerical simulation of high-dimensional possibly stiff dynamical systems. Designing such surrogate dynamical models can be formulated abstractly as a problem of function approximation under supervision: mapping a current state to a new state at a later point in time, using information of a given training data set. Being able to approximate this function with satisfactory accuracy then allows for forecasting by mapping unseen data. The concept of supervised learning can further be exploited to find computationally tractable reduced models for a subset of resolved variables. This problem arises in the context of multi-scale systems where one is typically interested in the dynamics of the slow resolved variables. Reducing a stiff potentially high-dimensional multi-scale system to an effective evolution equation for the slow variables only has obvious computational advantages, reducing the dimensionality and allowing for a larger time step in the numerical discretisation. In this context the aim of machine learning is to learn the so called closure term which parametrizes the effect of the fast unresolved degrees of freedom on the resolved slow dynamics. Ideally one aims at determining the closure term when only observations of the resolved variables are available.

A particularly simple and computationally cheap machine learning technique involves random feature maps (Rahimi and Recht, 2008). Akin to expressing functions as linear combination of basis functions in some Hilbert space such as for example Fourier or Chebychev basis functions, here functions are expressed as linear combinations of functions $\phi(\mathbf{w} \cdot \mathbf{u} + b)$, where \mathbf{w} and b are randomly drawn. It was shown that linear combinations of random feature maps are able to approximate continuous functions arbitrarily close, a property known as universal approximation property (Park and Sandberg, 1991; Cybenko, 1989; Barron, 1993). The task of training consists of learning the coefficients of the linear combination which can be achieved efficiently by linear ridge regression. See Rahimi and Recht (2008); Bach (2017a,b); Sun et al. (2019) for recent accounts. In the context of learning models of dynamical systems the framework of random feature maps was extended to include internal degrees of freedom with their own dynamics in so called echo-state networks (Maass et al., 2002; Jaeger, 2002; Jaeger and Haas, 2004; Pathak et al., 2018). Random feature maps and their extensions have been successfully used when the training data set is noise-free, e.g. when the data originate from a known underlying model. In the case when the model is unknown and the training data set instead consists of noisy observations, the architecture of random feature maps proves to be too sensitive to noise and is not able to provide a mapping to be used for forecasting unseen data.

To incorporate noisy observations to estimate the state of a dynamical system is a problem addressed by data assimilation (DA) or filtering (Majda and Harlim, 2012; Law et al., 2015; Reich and Cotter, 2015). In DA incoming noisy observations are optimally incorporated to increase the predictability of a given forecast model. DA can be used to estimate the state variables as well as unknown parameters of the model. DA now constitutes a standard tool in science and engineering and is used, for example, in numerical weather forecasting where it is the main driver for

the increased predictability enjoyed over the past decades. DA has already been used successfully in data-driven modelling where the forecast model is replaced by delay coordinates using Takens embedding and phase space reconstruction (Hamilton et al., 2016). Here we shall combine the random feature map architecture within a data assimilation procedure. The idea is to learn the coefficients of the linear combination of the random feature map approximation sequentially by updating them in time with incoming observations rather than performing linear regression on the entire training data set. The forecast model within the data assimilation procedure is given by the random feature map model itself. It should be noted, however, that the resulting combined state-parameter estimation problem is no longer linear. Within such a setting, an attractive DA framework is provided by ensemble Kalman filters (EnKF) where the statistical information needed for the Kalman filter is provided through a Monte Carlo approximation of an ensemble of model forecasts (Majda and Harlim, 2012; Law et al., 2015; Reich and Cotter, 2015). Such ensemble filters were shown to perform very well for nonlinear dynamical systems unlike the classical Kalman filter. We coin our methodology with the acronym RAFDA, standing for RAndom Feature maps and Data Assimilation. We shall consider three prototypical dynamical systems to numerically investigate RAFDA and to illustrate how RAFDA is able to extend the good forecast skills of classical random feature maps to the case of noisy training data. We consider the Lorenz-63 model, the Kuramoto-Sivashinsky equation and the multi-scale Lorenz-96 system to show how RAFDA achieves the goals we set out above. Besides an improved forecast skill of single trajectories compared to classical random feature maps, RAFDA naturally extends to probabilistic forecasting as it automatically generates an ensemble of initial conditions. We will see that our method generates reliable ensembles for which each ensemble member has equal probability of being closest to the truth. The former application concerned the case when we are seeking a cheap surrogate model, learned from noisy training data without any information about the underlying dynamical system. In the context of multi-scale systems scientists often know the form of the physical model for the resolved slow scales but lack detailed information about the closure term driving the physical model. For the Lorenz-96 multi-scale system we show that given noisy observations of the slow variables RAFDA can determine the closure term and can be used to perform subgrid-scale parametrization.

The paper is organised as follow. In Section 2 we develop our RAFDA methodology. In Section 3 we present applications to the Lorenz-63 model, where we test in particular for the dependency of the forecast skill on the length of the training data set, the noise level and the reservoir size. We further show that ensembles generated through the combined random feature map and data assimilation procedure provide reliable ensembles to be used in probabilistic ensemble forecasting. We further consider the Kuramoto-Sivashinsky equation as a paradigmatic model for spatio-temporal chaos in partial differential equations in Section 4. In Section 5 we consider the multi-scale

Lorenz-96 model and show that RAFDA can be used to learn closure models for the effective slow dynamics. We conclude in Section 6 with a discussion and an outlook.

2. COMPUTATIONAL METHODS

Consider a D -dimensional dynamical system

$$\dot{\mathbf{u}} = \mathcal{F}(\mathbf{u}), \quad (1)$$

which is observed at discrete times $t_n = n\Delta t$ of interval length $\Delta t > 0$, $n = 0, \dots, N$, to yield a noisy time series of vector-valued observations $\mathbf{u}_n^o \in \mathbb{R}^D$

$$\mathbf{u}_n^o = \mathbf{u}_n + \mathbf{\Gamma}^{1/2} \boldsymbol{\eta}_n \quad (2)$$

with measurement error covariance matrix $\mathbf{\Gamma} \in \mathbb{R}^{D \times D}$ and independent and normally distributed noise $\boldsymbol{\eta}_n \in \mathbb{R}^D$, that is, $\boldsymbol{\eta}_n \sim \mathcal{N}(\mathbf{0}, \mathbf{I})$. We will typically work with a measurement error covariance matrix

$$\mathbf{\Gamma} = \eta \mathbf{I} \quad (3)$$

with scalar variance parameter $\eta \geq 0$. The special case $\eta = 0$ corresponds to exact state observations. In this paper, we are primarily interested in noisy state observations, that is, in $\eta > 0$.

For the purpose of data-driven modelling and machine learning it is instructive to view the evolution of the time-dependent model state $\mathbf{u}(t)$ in the time interval Δt as a propagator map

$$\mathbf{u}_{n+1} = \Psi_{\Delta t}(\mathbf{u}_n). \quad (4)$$

The aim of data-driven modelling is then to find an approximation of this map and construct a surrogate model

$$\hat{\mathbf{u}}_{n+1} = \Psi_S(\hat{\mathbf{u}}_n) \quad (5)$$

with $\hat{\mathbf{u}}_0 = \mathbf{u}_0$, which is to be learned from the observational data (2). The observational data may come as outputs from a known model or are given by actual observations without any knowledge of the underlying model. In the case when the model is known a surrogate model may still have computational advantages, in particular for high-dimensional models and/or for stiff multi-scale models, where solving the full model may require too small step-sizes $\delta t \ll \Delta t$. One can also encounter the case when the underlying dynamics (1) is only partially known. This situation arises typically in multi-scale systems, where $\mathbf{u}(t)$ characterises the resolved (slow) degrees of freedom and the analytic form of \mathcal{F} is known but the effect of the unresolved dynamics on the resolved one has to be inferred from data.

Independent of whether the underlying model (1) is known or not, one ends up with a combined problem of having to estimate the states $\mathbf{u}_n \approx \mathbf{u}(t_n)$ as well as the functional form of the propagator Ψ_S from the noisy data \mathbf{u}_n^o , $n = 1, \dots, N$. This problem has been well studied in the literature, both within parametric and non-parametric settings, using different approximation tools such as radial basis functions (RBF) and reproducing kernel Hilbert spaces (RKHS). In this paper, we focus on a particular class of shallow neural networks and the RKHS induced by their random

feature maps. See, for example, Bach (2017a,b); Sun et al. (2019) for recent theoretical results on such approximations. In particular, the attractiveness of this RKHS, as compared to more complex machine learning architectures such as those considered for example in Qi and Majda (2020), is its easy embedding into sequential data assimilation via the ensemble Kalman filter (Evensen, 2006), as we will demonstrate in this paper.

The random feature approximation to (5) proceeds as follows: We define D_r feature maps, which we write in vector form as

$$\phi(\mathbf{u}) = \tanh(\mathbf{W}_{\text{in}}\mathbf{u} + \mathbf{b}_{\text{in}}) \quad (6)$$

using a weight matrix $\mathbf{W}_{\text{in}} \in \mathbb{R}^{D_r \times D}$ and a bias $\mathbf{b}_{\text{in}} \in \mathbb{R}^{D_r}$. The weight matrix and the bias are chosen randomly and independently of the observed \mathbf{u}_n^o , $n = 0, \dots, N$. The surrogate propagator (4) is then defined by

$$\Psi_S(\mathbf{u}) = \mathbf{W}\phi(\mathbf{u}), \quad (7)$$

where $\mathbf{W} \in \mathbb{R}^{D \times D_r}$ is a matrix of coefficients which will be learned from the data \mathbf{u}_n^o , $n = 0, \dots, N$. It was shown that random feature maps and their associated RKHS enjoy the universal approximation property (Park and Sandberg, 1991; Cybenko, 1989; Barron, 1993), stating that their associated RKHS are dense in the space of continuous functions. Their success in practical applications, however, depends crucially on an appropriate choice of two random sets of parameters \mathbf{W}_{in} and \mathbf{b}_{in} . We will comment on this aspect in more detail later.

Remark: Recently there has been a lot of interest in echo-state networks and reservoir computing (Jaeger, 2002; Jaeger and Haas, 2004; Pathak et al., 2018) which involve internal reservoir dynamics. Here we find that this additional complexity is not necessary to achieve good forecasting skill. Random feature maps have recently also been extended to solution maps of partial differential equations. See, for example, (Nelson and Stuart, 2020). All these contributions either assume exact state observations or ignore measurement errors.

2.1. Zero measurement noise: Linear Regression. If the measurement noise in (2) is zero, that is $\mathbf{u}_n = \mathbf{u}_n^o$, the external weight matrix $\mathbf{W} \in \mathbb{R}^{D \times D_r}$, which maps the random features to the state variable at the next time step, can be determined via linear ridge regression (LR) over a training data set of length N . More precisely, we seek the minimiser of

$$\mathcal{L}(\mathbf{W}) = \frac{1}{2} \|\mathbf{W}\Phi - \mathbf{U}^o\|_F^2 + \frac{\beta}{2} \|\mathbf{W}\|_F^2, \quad (8)$$

where $\|\mathbf{A}\|_F$ denotes the Frobenius norm of a matrix \mathbf{A} , $\mathbf{U}^o \in \mathbb{R}^{D \times N}$ is the matrix with columns \mathbf{u}_n^o , $n = 1, \dots, N$, and $\Phi \in \mathbb{R}^{D_r \times N}$ consists of columns

$$\phi_n = \phi(\mathbf{u}_{n-1}^o), \quad (9)$$

$n = 1, \dots, N$. The parameter $\beta \geq 0$ is used for regularization. The minimiser of (8), which we denote by \mathbf{W}_{LR} , is explicitly given by

$$\mathbf{W}_{\text{LR}} = \mathbf{U}^o \Phi^T (\Phi \Phi^T + \beta \mathbf{I})^{-1}. \quad (10)$$

We shall explore in Sections 3-5 in how far linear ridge regression can be used to construct a forecast model trained on noisy observations.

2.2. Non-zero measurement noise: RAFDA. If the observations are contaminated by noise, we propose here to estimate the weight matrix \mathbf{W} recursively using sequential DA (Majda and Harlim, 2012; Law et al., 2015; Reich and Cotter, 2015). Whereas the non-recursive estimation described in the previous Section using linear ridge regression only utilizes the information contained in the observations, we here aim at optimally estimating the weight matrix using both the observations as well as the underlying dynamical surrogate model (5). In particular, we employ a combined state and parameter estimation via state augmentation (Majda and Harlim, 2012; Reich and Cotter, 2015). More precisely, we formulate the forecast model for constant parameters \mathbf{W} as

$$\mathbf{u}_{n+1}^f = \mathbf{W}_n^a \phi(\mathbf{u}_n^a) \quad (11a)$$

$$\mathbf{W}_{n+1}^f = \mathbf{W}_n^a, \quad (11b)$$

where the superscript f denotes the forecast and the superscript a denotes the analysis defined below. Furthermore, the model states \mathbf{u}_n^a , \mathbf{W}_n^a and \mathbf{u}_{n+1}^f , \mathbf{W}_{n+1}^f , respectively, are now treated as random variables. To formulate the Kalman filter analysis step, we unravel the weight matrix $\mathbf{W} \in \mathbb{R}^{D \times D_r}$ into a parameter vector $\mathbf{w} \in \mathbb{R}^{DD_r}$ with $w_{1:D_r} = W_{11}, \dots, W_{1D_r}$, $w_{D_r+1:2D_r} = W_{21}, \dots, W_{2D_r}$ and so forth. Concatenating further we introduce $\mathbf{z} = (\mathbf{u}^T, \mathbf{w}^T)^T \in \mathbb{R}^{D_z}$ with $D_z = D + DD_r$. While the forecast step (11) leads to an update of the random variable \mathbf{z}_n^a into \mathbf{z}_{n+1}^f , the analysis step for the mean is provided by

$$\bar{\mathbf{z}}_{n+1}^a = \bar{\mathbf{z}}_{n+1}^f - \mathbf{K}_{n+1}(\mathbf{H}\bar{\mathbf{z}}_{n+1}^f - \mathbf{u}_{n+1}^o) \quad (12)$$

with the observation matrix $\mathbf{H} \in \mathbb{R}^{D \times D_z}$ defined by $\mathbf{H}\mathbf{z} = \mathbf{u}$, i.e. we assume that we observe all state variables \mathbf{u} . The Kalman gain matrix \mathbf{K} is given by

$$\mathbf{K}_{n+1} = \mathbf{P}_{n+1}^f \mathbf{H}^T (\mathbf{H} \mathbf{P}_{n+1}^f \mathbf{H}^T + \Gamma)^{-1}, \quad (13)$$

where the forecast covariance matrix is given by

$$\mathbf{P}_{n+1}^f = \langle \hat{\mathbf{z}}_{n+1}^f \otimes \hat{\mathbf{z}}_{n+1}^f \rangle = \begin{pmatrix} \langle \hat{\mathbf{u}}_{n+1}^f \otimes \hat{\mathbf{u}}_{n+1}^f \rangle & \langle \hat{\mathbf{u}}_{n+1}^f \otimes \hat{\mathbf{w}}_{n+1}^f \rangle \\ \langle \hat{\mathbf{w}}_{n+1}^f \otimes \hat{\mathbf{u}}_{n+1}^f \rangle & \langle \hat{\mathbf{w}}_{n+1}^f \otimes \hat{\mathbf{w}}_{n+1}^f \rangle \end{pmatrix}. \quad (14)$$

The angular brackets $\langle f(\mathbf{z}) \rangle$ denote the expectation value of a function $f(\mathbf{z})$ and the hat denotes the perturbation of \mathbf{z}_{n+1}^f from its mean $\bar{\mathbf{z}}_{n+1}^f = \langle \mathbf{z}_{n+1}^f \rangle$, that is,

$$\hat{\mathbf{u}}_{n+1}^f = \mathbf{u}_{n+1}^f - \bar{\mathbf{u}}_{n+1}^f. \quad (15)$$

Since we are only observing the state variables \mathbf{u} , the Kalman update (12) can be written to explicitly separate the state and parameter variables as

$$\bar{\mathbf{u}}_{n+1}^a = \bar{\mathbf{u}}_{n+1}^f - \mathbf{P}_{uu}^f (\mathbf{P}_{uu}^f + \Gamma)^{-1} (\bar{\mathbf{u}}_{n+1}^f - \mathbf{u}_{n+1}^o) \quad (16)$$

$$\bar{\mathbf{w}}_{n+1}^a = \bar{\mathbf{w}}_{n+1}^f - \mathbf{P}_{wu}^f (\mathbf{P}_{uu}^f + \Gamma)^{-1} (\bar{\mathbf{u}}_{n+1}^f - \mathbf{u}_{n+1}^o), \quad (17)$$

where $\mathbf{P}_{uu}^f = \langle \hat{\mathbf{u}}_{n+1}^f \otimes \hat{\mathbf{u}}_{n+1}^f \rangle$ and $\mathbf{P}_{wu}^f = \langle \hat{\mathbf{w}}_{n+1}^f \otimes \hat{\mathbf{u}}_{n+1}^f \rangle$.

The Kalman filter is optimal in the sense that $\bar{\mathbf{z}}^a$ maximizes the likelihood of the observations provided that both the observations and the state variables are Gaussian distributed random variables. Since the forward model (11) is nonlinear in the augmented state variable and the involved random variables cannot assumed to be Gaussian distributed, the combined forecast and analysis cycle is not well defined and we employ the stochastic EnKF (Burgers et al., 1998; Evensen, 2006) to define a computationally robust Monte Carlo closure. In particular, define an ensemble of states $\mathbf{Z} \in \mathbb{R}^{D_z \times M}$ consisting of M members $\mathbf{z}^{(i)} \in \mathbb{R}^{D_z}$, $i = 1, \dots, M$, that is,

$$\mathbf{Z} = [\mathbf{z}^{(1)}, \mathbf{z}^{(2)}, \dots, \mathbf{z}^{(M)}], \quad (18)$$

their empirical mean

$$\bar{\mathbf{z}} = \frac{1}{M} \sum_{i=1}^M \mathbf{z}^{(i)}, \quad (19)$$

and the associated matrix of ensemble deviations

$$\hat{\mathbf{Z}} = [\mathbf{z}^{(1)} - \bar{\mathbf{z}}, \mathbf{z}^{(2)} - \bar{\mathbf{z}}, \dots, \mathbf{z}^{(M)} - \bar{\mathbf{z}}] \in \mathbb{R}^{D_z \times M}. \quad (20)$$

We define these objects for the forecast and analysis ensembles \mathbf{Z}_n^f and \mathbf{Z}_n^a , respectively, for all $n \geq 0$. Each ensemble member is propagated individually under the forecast step (11). This defines the update from the last analysis ensemble \mathbf{Z}_n^a to the next forecast ensemble \mathbf{Z}_{n+1}^f . The EnKF analysis step is now defined as follows. The ensemble deviation matrix $\hat{\mathbf{Z}}_{n+1}^f$ can be used to approximate the forecast covariance matrix (14) as

$$\mathbf{P}_{n+1}^f = \frac{1}{M-1} \hat{\mathbf{Z}}_{n+1}^f (\hat{\mathbf{Z}}_{n+1}^f)^T \in \mathbb{R}^{D_z \times D_z}. \quad (21)$$

Upon introducing the matrix $\mathbf{U}_{n+1}^o \in \mathbb{R}^{D \times M}$ of perturbed observations

$$\mathbf{U}_{n+1}^o = [\mathbf{u}_{n+1}^o - \Gamma^{1/2} \boldsymbol{\eta}_{n+1}^{(1)}, \mathbf{u}_{n+1}^o - \Gamma^{1/2} \boldsymbol{\eta}_{n+1}^{(2)}, \dots, \mathbf{u}_{n+1}^o - \Gamma^{1/2} \boldsymbol{\eta}_{n+1}^{(M)}], \quad (22)$$

where the $\boldsymbol{\eta}_{n+1}^{(i)} \in \mathbb{R}^D$, $i = 1, \dots, M$, are realisations of independent and normally distributed random variables (compare (2)), we obtain the following compact representation of the EnKF update step:

$$\mathbf{Z}_{n+1}^a = \mathbf{Z}_{n+1}^f - \mathbf{P}_{n+1}^f \mathbf{H}^T (\mathbf{H} \mathbf{P}_{n+1}^f \mathbf{H}^T + \Gamma)^{-1} (\mathbf{H} \mathbf{Z}_{n+1}^f - \mathbf{U}_{n+1}^o). \quad (23)$$

The ensemble forecast step defined by (11), together with the EnKF analysis step (23) constitute our combined RANdom Features maps and Data Assimilation

(RAFDA) method. The resulting weight matrix \mathbf{W}_N^a at final training time N is denoted by $\mathbf{W}_{\text{RAFDA}}$.

In the subsequent two subsections we discuss further algorithmic details of our method.

2.3. Choice of random feature maps. The choice of the random coefficients \mathbf{b}_{in} and \mathbf{W}_{in} in the feature maps (6) and their dimension D_r is crucial for the success of our method. In this study, we choose these entries to be independent and uniformly distributed with

$$(\mathbf{W}_{\text{in}})_{ij} \sim \mathcal{U}[-w, w] \quad \text{and} \quad (\mathbf{b}_{\text{in}})_i \sim \mathcal{U}[-b, b]. \quad (24)$$

The hyper-parameters $w > 0$ and $b > 0$ should be chosen such that the random feature maps (9) evaluated at the observed data points cover their full range of $[-1, 1]^D$ as uniformly as possible, in particularly sampling their nonlinear domain. See the numerical experiment section for more details.

We mention that one could also dynamically adapt those parameters. This would extend our method from random feature maps to two-layer networks, going from RKHS to Barron spaces (Chizat and Bach, 2018; Mei et al., 2018; Rotskoff and Vanden-Eijnden, 2018; Sirignano and Spiliopoulos, 2020; E et al., 2019). We leave this option in combination with data assimilation as a topic for further research.

2.4. Further algorithmic details of RAFDA. The required ensemble size M of the standard implementation (23) of an EnKF has to be of the order $\mathcal{O}(D_z)$, which can become prohibitive for typical reservoir sizes of $D_r \sim \mathcal{O}(10^3)$ and potentially high-dimensional dynamical systems. Within the EnKF community further approximations such as localisation and inflation have been developed to deal with finite-size effects (Evensen, 2006; Reich and Cotter, 2015; Houtekamer and Zhang, 2016). Here we follow the concept of B-localisation (Houtekamer and Mitchell, 1998, 2001; Hamill et al., 2001), where the empirical covariance matrix \mathbf{P}_{n+1}^f is tempered by a symmetric positive definite localisation matrix \mathbf{B} via the Kronecker product, that is,

$$\tilde{\mathbf{P}}_{n+1}^f = \mathbf{B} \circ \mathbf{P}_{n+1}^f. \quad (25)$$

The EnKF update step (23) is then replaced by

$$\mathbf{Z}_{n+1}^a = \mathbf{Z}_{n+1}^f - \tilde{\mathbf{P}}_{n+1}^f \mathbf{H}^T \left(\mathbf{H} \tilde{\mathbf{P}}_{n+1}^f \mathbf{H}^T + \mathbf{\Gamma} \right)^{-1} \left(\mathbf{H} \mathbf{Z}_{n+1}^f - \mathbf{U}_{n+1}^o \right). \quad (26)$$

Localisation implies that certain correlations between variables get reduced or even set to zero if the corresponding entry in \mathbf{B} is less than one or zero, respectively. This allows to control spurious correlations between uncorrelated variables of $\mathcal{O}(1/\sqrt{M})$, caused by employing a finite ensemble size. In our numerical experiments we employ the following form of localisation. The j th row of the weight matrix \mathbf{W} is responsible for updating the j th component of the dynamic state variable \mathbf{u} under the forward model (11a). We reflect this property in the approximate covariance matrix $\tilde{\mathbf{P}}_{n+1}^f$

by ignoring all correlations between the j th row of \mathbf{W} and all components of the observed \mathbf{u}_{n+1}^o except for its j th entry.

We also employ multiplicative inflation in which the members $\mathbf{z}_{n+1}^{(i)}$ of the forecast ensemble \mathbf{Z}_{n+1}^f are replaced by

$$\mathbf{z}_{n+1}^{(i)} \rightarrow \bar{\mathbf{z}}_{n+1} + \alpha(\mathbf{z}_{n+1}^{(i)} - \bar{\mathbf{z}}_{n+1}), \quad (27)$$

$i = 1, \dots, M$, prior to the EnKF data assimilation step (23) with $\alpha > 1$ being the inflation factor (Anderson and Anderson, 1999). Note that the inflation step maintains the ensemble mean while increasing the covariance matrix \mathbf{P}_{n+1}^f of the ensemble.

We finally need to specify the distribution of the extended state variable \mathbf{z} at initial time $t = 0$. We treat the two components \mathbf{u}_0 and \mathbf{w}_0 of \mathbf{z}_0 as independent and set

$$\mathbf{u}_0 \sim \mathcal{N}(\mathbf{u}_0^o, \mathbf{\Gamma}) \quad (28)$$

as well as

$$\mathbf{w}_0 \sim \mathcal{N}(\mathbf{w}_{\text{LR}}, \gamma \mathbf{I}), \quad (29)$$

where \mathbf{w}_{LR} is the vectorial form of the solution \mathbf{W}_{LR} to the ridge regression formulation (8) and $\gamma > 0$ is a parameter. Alternatively, one can also use $\mathbf{w}_0 \sim \mathcal{N}(\mathbf{0}, \gamma \mathbf{I})$ if \mathbf{w}_{LR} is unavailable.

In the subsequent sections we illustrate the proposed RAFDA methodology in several dynamical systems, demonstrate its improved forecast skill compared to the linear regression approach (10), and investigate the dependency of RAFDA on the noise strength and the available training size N , as well as showing the impact on the approximation properties of RAFDA of the various choices a modeller needs to take such as the reservoir dimension D_r and the choice of the random elements \mathbf{W}_{in} and \mathbf{b}_{in} .

3. ORDINARY DIFFERENTIAL EQUATIONS: LORENZ-63 EQUATION

We consider as a first test bed the Lorenz-63 system (Lorenz, 1963)

$$\begin{aligned} \dot{y} &= 10(y - x) \\ \dot{x} &= 28x - y - xz \\ \dot{z} &= -\frac{8}{3}z + xy \end{aligned} \quad (30)$$

with $\mathbf{u} = (x, y, z)^T \in \mathbb{R}^3$. Observations are taken every $\Delta t = 0.02$ time units and \mathbf{u}_n corresponds to the solution at $t_n = n\Delta t$. In all simulations a transient of 40 time units is discarded to ensure that the dynamics has settled on the attractor.

To assess the propensity of random feature maps with data assimilation and classical random feature maps with linear regression to be used as a forecast model we test the forecast models of LR

$$\mathbf{u}_{n+1} = \mathbf{W}_{\text{LR}}\phi(\mathbf{u}_n) \quad (31)$$

with \mathbf{W}_{LR} given by (10), and of RAFDA

$$\mathbf{u}_{n+1} = \mathbf{W}_{\text{RAFDA}}\phi(\mathbf{u}_n), \quad (32)$$

where $\mathbf{W}_{\text{RAFDA}}$ is determined via the training data as the final outcome of the iterative DA procedure given by (11) and (23). In both cases the reservoir variables are given by (6). For LR we employ a regularization parameter of $\beta = 0.001$. For RAFDA we do not use inflation ($\alpha = 0$) and set, unless stated otherwise, $D_r = M = 300$ and $N = 4,000$ and a noise strength of $\eta = 0.2$.

We test the respective forecast capabilities in a validation data set $\mathbf{u}_{\text{valid}}(t_n)$, $n \geq 0$. As a quantitative diagnostic for the forecast skill we record the forecast time τ_f , defined as the largest time such that the relative forecast error $\mathcal{E}(t_n) = \|\mathbf{u}_{\text{valid}}(t_n) - \mathbf{u}_n\|^2 / \|\mathbf{u}_{\text{valid}}(t_n)\|^2 \leq \theta$. We choose here $\theta = 0.05$. We measure time in units of the Lyapunov time $t\lambda_{\text{max}}$ with the maximal Lyapunov exponent $\lambda_{\text{max}} = 0.91$. In the following we discuss the effect of the various parameters as well as on the length of the available data and the noise levels on the forecast capabilities of the two models.

3.1. Dependency on the internal parameters. We first address the issue of the choice of the randomly chosen internal parameters \mathbf{W}_{in} and \mathbf{b}_{in} . The entries of the internal weight matrix and bias are chosen uniformly randomly over intervals $[-w, w]$ in case of \mathbf{W}_{in} and $[-b, b]$ in case of \mathbf{b}_{in} (cf (24)). Figure 1 shows the forecast times τ_f as a function of the two parameters w and b for single realisations of (24). The forecast times are estimated using the ridge linear regression matrix \mathbf{W}_{LR} for a single time series of noiseless observations with $N = 200,000$ training data points. Results are shown for training on noiseless and on noisy observations with $\eta = 0.2$. The forecast capabilities clearly depend sensitively on the choice of w and b . In particular, parameter choices leading to excellent forecast times in the noiseless case may not lead to good forecast times in the case of non-zero measurement noise. To explore what constitutes a good set of inner parameters corresponding to long forecast times we show in Figure 2 normalized histograms of one of the components of the random feature map ϕ_j (cf (6)). For inner parameter choices corresponding to poor forecast times $\tau_f < 0.5$ the histograms exhibit strongly localised behaviour near ± 1 , caused by the tanh-random feature map (6) having scale parameters w such that the tanh-function cannot resolve the whole range of dynamical states of the underlying observations. Inner parameters corresponding to long forecast times on the other hand resolve the whole dynamical range within the nonlinear range of the tanh-function. In the following the internal weight matrix and bias are chosen randomly with $w = 0.005$ and $b = 4$ which yields large forecast times τ_f for $\eta = 0$ and $\eta = 0.2$ (cf. Figure 1).

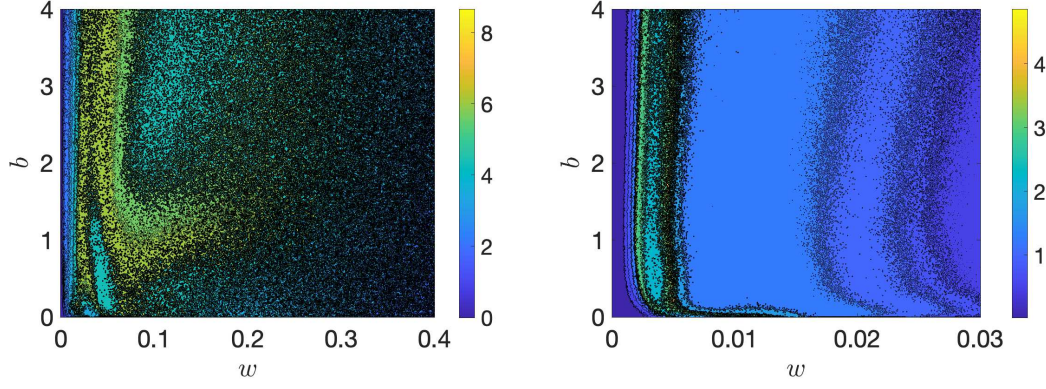


FIGURE 1. Contourplot of the forecast time τ_f for different choices of the internal parameters and measurement noise variance η . Left: $\eta = 0$. Right: $\eta = 0.2$

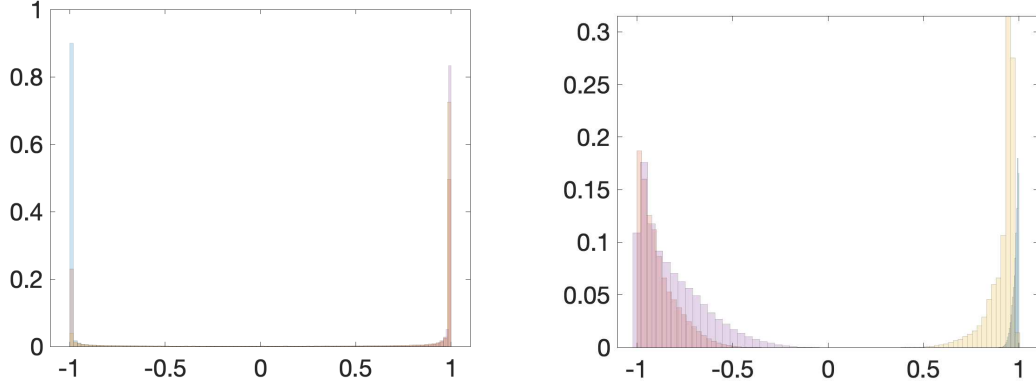


FIGURE 2. Normalized empirical histogram of the random feature map (6) ϕ_1 for four choices of inner parameters w and b . Left: inner parameters corresponding to forecast times $\tau_f < 0.5$. Right: inner parameters corresponding to forecast times $\tau_f > 6$.

3.2. Dependency of LR on the regularization parameter β . Figure 3 shows the mean of the forecast time τ_f obtained from LR for size $D_r = 300$ for different choices of the regularization parameter β , averaged over 500 realisations, each trained on $N = 4,000$ observations. We observe that when noiseless data are used to train LR, the forecast time has a maximum for $\beta = 2.5 \cdot 10^{-8}$. For noisy observations with $\eta = 0.2$ the mean forecast time τ_f is relatively robust to changes in the regularization parameter for a wide range of β .

3.3. Dependency of RAFDA on the initial ensemble. Turning to RAFDA, we now investigate the influence on the choice of the initial ensemble for the parameters. We consider initial ensembles drawn in an unbiased fashion $\mathbf{w}_0 \sim \mathcal{N}(\mathbf{0}, \gamma \mathbf{I})$ as well as

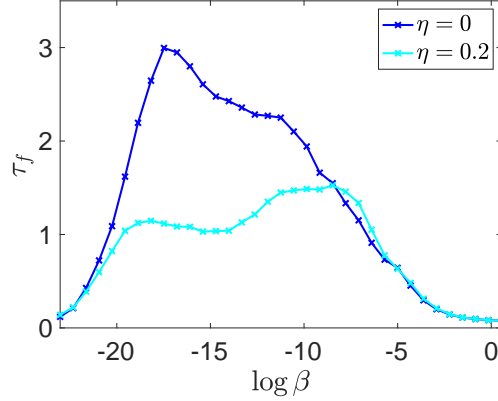


FIGURE 3. Mean of the forecast time τ_f in units of the Lyapunov time for varying regularization parameters β for LR for noiseless ($\eta = 0$) and for noise contaminated observations ($\eta = 0.2$).

drawn around the prior provided by LR $\mathbf{w}_0 \sim \mathcal{N}(\mathbf{w}_{\text{LR}}, \gamma \mathbf{I})$ as in (29), where we employ $\beta = 2.5 \cdot 10^{-8}$ to obtain \mathbf{w}_{LR} (which gave rise to the peak in the forecast time for noiseless data; cf. Figure 3). The model is trained on $N = 4,000$ noisy observations with noise level $\eta = 0.2$ and a reservoir of dimension $D_r = 300$ was used. We chose $M = 300$ ensemble members for RAFDA, and averaged over 500 realisations. Figure 4 shows the dependency of the mean forecast time on the initial spread of the ensemble γ . For both types of initial ensembles there is a wide range of initial ensemble spreads γ for which good forecast times are obtained. As to be expected, the same forecast times τ_f are produced for large values of γ independent if the initial ensemble was chosen centred around the prior \mathbf{W}_{LR} or unbiased. Centering the initial ensemble around the prior provided by LR produces larger forecast times than LR for noisy data for $\gamma > 2.5 \cdot 10^{-4}$, and generally leads to more robust forecast times with respect to the initial spread γ than the unbiased initial ensemble. We remark that the differences between the two initialisation choices depend on the noise level of the training data set; for small noise levels, centering the initial ensemble around the prior provided by LR leads to better forecast times compared to the unbiased initial ensemble for a wider range of values of γ . In the following we will use initial ensembles centred around the prior provided by LR with $\gamma = 1,000$.

3.4. Dependency on the reservoir dimension D_r . Figure 5 shows the dependency of the forecast time τ_f on the reservoir dimension D_r for fixed training length $N = 4,000$. For each reservoir size we choose an ensemble with $M = D_r$ members. The forecast performance of both RAFDA and LR increases with the reservoir size D_r initially and then saturates for sufficiently large D_r . In the saturated range the forecast times of RAFDA are almost twice as large as classical LR.

Figure 6 shows the empirical histogram of the forecast time τ_f for RAFDA and for LR over 500 independent realisations. RAFDA clearly exhibits improved forecast

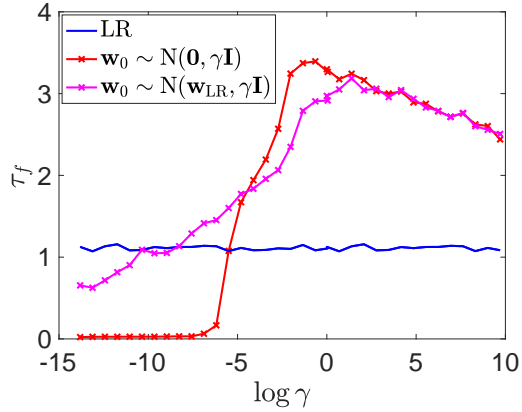


FIGURE 4. Mean of the forecast time τ_f in units of the Lyapunov time for varying γ for RAFDA for noise contaminated observations with $\eta = 0.2$. Shown are results when the initial ensemble is drawn around the prior provided by LR $\mathbf{w}_0 \sim N(\mathbf{w}_{LR}, \gamma \mathbf{I})$ (29) and the unbiased choice $\mathbf{w}_0 \sim N(\mathbf{0}, \gamma \mathbf{I})$. For each realisation the prior is calculated anew, leading to a slightly jagged curve for LR.

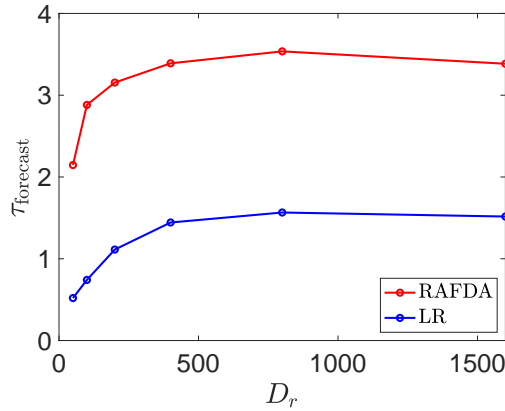


FIGURE 5. Mean of the forecast time τ_f in units of the Lyapunov time for varying reservoir size D_r for RAFDA and for LR.

times with a mean of 3.9 time units over LR with a mean of 2.2 time units. We used here a reservoir of size $D_r = 1,600$ with $M = 1,600$ ensemble members. The models are trained with $N = 4,000$ noisy observations.

3.5. Dependency on the training data size N . The size of the training data set needs to be sufficiently large for two separate reason. First of all, the training data set needs to sample sufficient parts in phase space to allow for forecasting of unseen data which may explore different areas of phase space. Secondly, the size of the training data set needs to be sufficiently large to allow for good statistical estimation

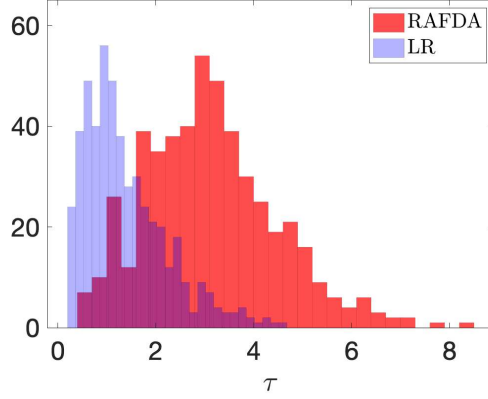


FIGURE 6. Empirical histogram of forecast times τ_f in units of the Lyapunov time for $D_r = 1,600$.

of both LR and DA (which has its own initial transient period) and to allow for a finer estimation of the mapping (31) and (32), respectively.

Figure 7 shows the dependency of the mean of the forecast time τ_f on the size N of a noisy training data set over 500 independent validation data sets. We checked that the analysis fields for the Lorenz-63 system variables were close to the truth and no ensemble inflation was required. As for the reservoir dimension, the forecast times τ_f increase with increasing length of the training data set N and saturate for sufficiently large training data sets, exhibiting the same twofold improvement of RAFDA over LR as observed in Section 3.4.

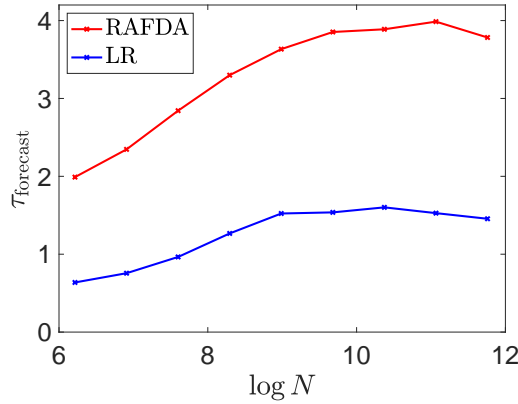


FIGURE 7. Mean of the forecast time τ_f in units of the Lyapunov time for varying lengths N of the training data set for RAFDA and for LR.

3.6. Dependency on the measurement noise level η . We now test how the forecast capabilities depend on the observational noise level η . Figure 8 shows the

dependency of the forecast time τ_f on the noise level for fixed training data length and reservoir dimension. For sufficiently small noise levels $\eta < 0.0004$ RAFDA asymptotes to a mean forecast time of $\tau_f \approx 5.3$ whereas LR asymptotes to only $\tau_f \approx 1.8$, albeit for a longer range in noise levels. The range of constant forecast times is followed by an exponentially decaying range, before the models loose any forecast skill with $\tau_f \rightarrow 0$. The exponential behaviour of the forecast time τ_f with respect to the observational noise strength η is consistent with the sensitivity of chaotic dynamical systems with respect to their initial condition and the exponential separation of nearby trajectories. To corroborate this interpretation we have confirmed that the same forecast times are achieved when simultaneously doubling the data size to $N = 8,000$ and the noise level η .

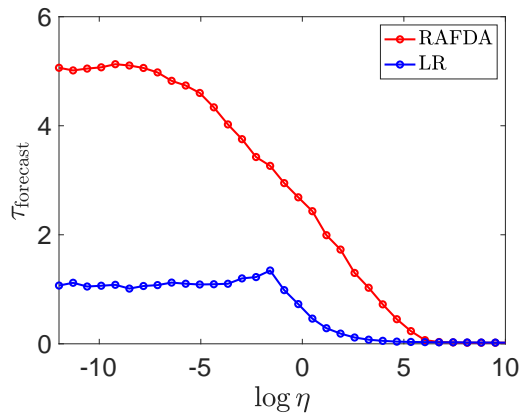


FIGURE 8. Mean of the forecast time τ_f in units of the Lyapunov time for varying noise levels η for RAFDA and for LR.

3.7. Application to ensemble forecasting. In chaotic dynamical systems a single forecast is to a certain degree meaningless as small uncertainties in the initial condition can lead to widely differing forecasts at a later time. Probabilistic forecasts provide a more appropriate framework for forecasting. In particular, ensemble forecasting, whereby a Monte Carlo estimate of the underlying probability density function is provided by running an ensemble of initial conditions, are now widely used in numerical weather forecasting issuing both the most probable forecast and its associated uncertainty (Epstein, 1969; Leith, 1974; Leutbecher and Palmer, 2008). The quality of such ensemble forecasts crucially depends on how the ensembles are generated. There exist several strategies using singular vectors (Lorenz, 1965; Palmer, 1993), bred vectors (Toth and Kalnay, 1993, 1997; Giggins and Gottwald, 2019), analysis ensembles from ensemble Kalman filters (Wang and Bishop, 2003; Buizza et al., 2005), and more recently analogs (Atencia and Zawadzki, 2017). Here we show that ensembles obtained from RAFDA provide reliable forecast ensembles to be used in probabilistic forecasts. A good probabilistic forecasts is not necessarily one with the smallest

root-mean-square (RMS) error (consider a probability density function with disjoint support, then the mean may not be even an actual physical state), but rather one where each ensemble member has equal probability of being closest to the truth. Such ensembles are called reliable. We probe the reliability here with the continuous ranked probability score (CRPS) (Hersbach, 2000; Wilks, 2006). The CRPS is defined for a lead time τ as

$$\text{CRPS}(\tau) = \frac{1}{D} \sum_{k=1}^D \int_{-\infty}^{\infty} \left[F(u; \tau, k) - F_{\text{truth}}(u; \tau, k) \right]^2 du, \quad (33)$$

where F and F_{truth} are the cumulative probability distributions of the forecast ensemble and truth, respectively, which are estimated as

$$F(u; \tau, k) = \frac{1}{M} \sum_{m=1}^M \Theta\left(u - u^{(m,k)}(\tau)\right), \quad (34)$$

$$F_{\text{truth}}(u; \tau, k) = \Theta\left(u - u_{\text{truth}}^{(k)}(\tau)\right), \quad (35)$$

where $\Theta(x)$ is the Heaviside function with $\Theta(x) = 0$ for $x < 0$ and $\Theta(x) = 1$ otherwise, and $u^{(m,k)}(\tau)$ denotes the k -component of the m th ensemble member $\mathbf{u}^{(m)}(\tau)$ at forecast time $\tau > 0$.

We consider here ensembles obtained through an EnKF data assimilation where the forecast model is comprised from either RAFDA or from LR. Both forecast models and their associated weight matrices were obtained prior to and independently from the data assimilation cycles using a training set of length $N = 250,000$, consisting of noisy observations with $\eta = 0.2$. We further compare with results obtained from a traditional EnKF ensemble where the full Lorenz-63 model (30) is employed as forecast model. We find that RAFDA provides the smallest RMS error with 0.1. The full EnKF yields an analysis RMS error of 0.17. LR has a markedly larger analysis RMS error of 7.8. Figure 9 shows $\text{CRPS}(\tau)$, averaged over 500 realisations, for the three ensembles. For small lead times EnKF and RAFDA perform similar. However, RAFDA clearly generates a more reliable ensemble for larger lead times. LR ensembles cannot be classified as reliable.

4. PARTIAL DIFFERENTIAL EQUATIONS: KURAMOTO-SIVASHINSKY EQUATION

We now consider artificially generated time series obtained from a numerical simulation of the Kuramoto-Sivashinsky equation (Kuramoto and Tsuzuki, 1975, 1976; Sivashinsky, 1977; Sivashinsky and Michelson, 1980)

$$u_t + uu_x + \alpha u_{xx} + u_{xxx} = 0 \quad (36)$$

with periodic boundary conditions. For system length $L = 22$ the Kuramoto-Sivashinsky equation is chaotic with a maximal Lyapunov exponent of $\lambda_{\text{max}} = 0.043$ (Edson et al., 2019). We remark that although the Kuramoto-Sivashinsky equation is

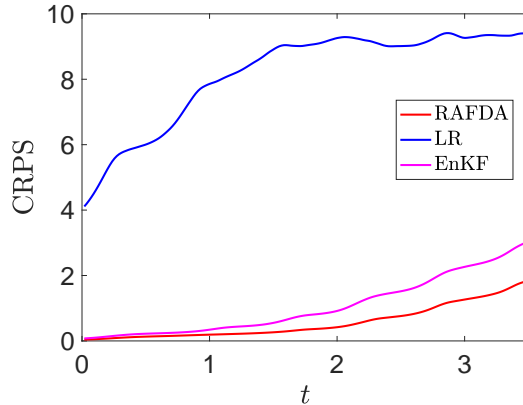


FIGURE 9. CRPS as a function of the lead time τ for RAFDA, LR and EnKF ensembles.

a partial-differential equation, its dynamics evolves on a finite dimensional manifold (Temam, 1997).

We generate observations \mathbf{u}_n^o by integrating (36) using a pseudo-spectral Crank-Nicolson scheme where the nonlinearity is treated with a second-order Adams-Bashforth scheme. We employ a temporal discretization step of $\delta t = 0.001$ and use 64 spatial grid points, and sample every $\Delta t = 0.25$ time units to obtain observations $\mathbf{u}_n^o \in \mathbb{R}^{64}$. An initial transient period of 25×10^6 time units is discarded to ensure that the dynamics has settled onto the attractor.

The internal weight matrix and bias are chosen randomly according to (24) with $w = 0.1$ and $b = 1$ with a reservoir of size $D_r = 2,000$. We train RAFDA on a noisy training data set of length $N = 70,000$ with $\eta = 0.01$. The data assimilation component of RAFDA was executed with $M = 1,000$ ensemble members and without any inflation with an initial ensemble chosen according to (29) with $\gamma = 6.4 \cdot 10^{-6}$. Figure 10 depicts results of the RAFDA forecast showing that reasonable forecasts can be made up to times close to four Lyapunov times. Classical random feature maps with linear ridge regression trained on the same data set only yield forecast horizons of one Lyapunov time. If LR is trained on noiseless data, it achieves comparable forecast skill to RAFDA. We have refrained here from optimizing the reservoir weights w and b and the reservoir dimension D_r to achieve larger forecast horizons.

5. CLOSURE MODELS: MULTI-SCALE LORENZ-96 SYSTEM

We consider now the problem of model closure in multi-scale systems. Typically one is only interested in the dynamics of the large-scale slow variables. Moreover, one typically only has access to observations of the resolved slow dynamics. The objective of model closure, or also known as the parametrization problem, is to find a self-consistent dynamical model for the resolved slow large-scale variables. The effective model for the slow large-scale dynamics allows for a larger time step in the

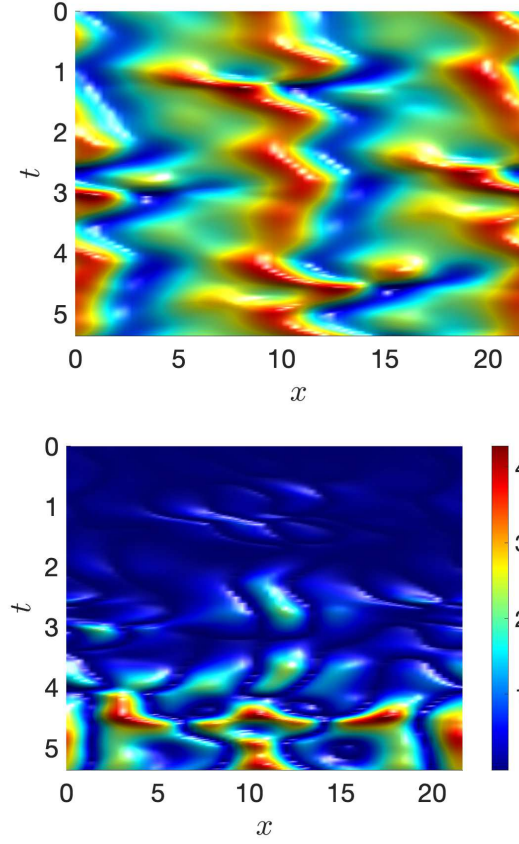


FIGURE 10. Hovmöller diagram of the forecast field $u(x, t)$. Left: RAFDA forecast. Right: Root-mean-square error of the RAFDA forecast and the truth. Times are in units of $1/\lambda_{\max}$.

numerical simulation compared to the prohibitively small time steps required in the full stiff multi-scale system.

We consider here the multi-scale Lorenz-96 system for K slow variables $X^{(k)}$ which are each coupled to J fast variables $Y^{(j,k)}$, given by

$$\frac{d}{dt}X^{(k)} = -X^{(k-1)}(X^{(k-2)} - X^{(k+1)}) - X^{(k)} + F - \frac{hc}{d} \sum_{j=1}^J Y^{(j,k)}, \quad (37)$$

$$\frac{d}{dt}Y^{(j,k)} = -cbY^{(j+1,k)}(Y^{(j+2,k)} - Y^{(j-1,k)}) - cY^{(j,k)} + \frac{hc}{d}X^{(k)}, \quad (38)$$

with cyclic boundary conditions $X^{(k+K)} = X^{(k)}$, $Y^{(j,k+K)} = Y^{(j,k)}$ and $Y^{(j+J,k)} = Y^{(j,k+1)}$, giving a total of $D = K(J+1)$ variables. This set of equations was introduced as a caricature for the midlatitude atmosphere (Lorenz, 1996). The variables $X^{(k)}$ model large scale atmospheric fields arranged on a latitudinal circle, such as synoptic weather systems. Each of the $X^{(k)}$ variables is connected to J small-scale variables

$Y^{(j,k)}$. The time scale separation is parametrized by the coefficient c , and the ratio of the amplitudes of the large-scale and the small-scale variables is controlled by b . The coupling between the slow and fast variables is controlled by the parameter h . Both large-scale and small-scale dynamics variables evolve when uncoupled according to nonlinear transport and linear damping; the large-scales are subjected to external forcing F . We choose here as parameters $K = 8$ and $J = 32$, leading to a total of 256 variables, and $F = 20$, $c = d = 10$ and $h = 1$ as in Wilks (2005); Arnold et al. (2013). The choice $c = d = 10$ implies that the variables $Y^{(j,k)}$ fluctuate with a 10 times higher frequency and with an approximately 10 times smaller amplitude when compared to the $X^{(k)}$. Setting the coupling constant $h = 1$, corresponds to strong coupling where the dynamics is driven by the fast sub-system (Herrera et al., 2010).

Our aim is to provide a reduced model of the form

$$\frac{d}{dt}X^{(k)} = G^{(k)}(\mathbf{X}) + \psi(X^{(k)}), \quad (39)$$

with $\mathbf{X} = (X^{(1)}, \dots, X^{(K)})^T$, $G^{(k)}(\mathbf{X}) = -X^{(k-1)}(X^{(k-2)} - X^{(k+1)}) - X^{(k)} + F$, and where the closure term $\psi(x)$ parametrizes the effect of the fast unresolved dynamics and is learned by RAFDA. Note that one and the same closure map can be applied at all grid points due to the spatial homogeneity of the problem. The application we have in mind is that a scientist has available a physics-based model for the resolved slow large-scale dynamics, but does not have access to the unresolved fast small-scale model, and the closure model needs to be inferred from noisy observations.

In the case when the full multi-scale model (37)–(38) is available and noiseless data of both the slow and fast variables are available, the closure problem has been attempted outside the scope of machine learning in Wilks (2005) and Arnold et al. (2013). Therein deterministic parametrizations were proposed by polynomial data-fitting the closure term to the resolved variables with

$$\psi_{\text{Wilks}}(x) = 0.262 + 1.45x - 0.0121x^2 - 0.00713x^3 + 0.000296x^4 \quad (40)$$

$$\psi_{\text{AMP}}(x) = 0.341 + 1.3x - 0.0136x^2 - 0.00235x^3. \quad (41)$$

Here we assume we are only given observations of the slow variables \mathbf{X}_n at discrete times $t_n = n\Delta t$. In LR, we set $\mathbf{u}_n = \mathbf{X}_n$, $n = 0, \dots, N$, and the closure mapping $\psi(x)$ is learned directly from the data via finite-differencing. More specifically, the closure is performed by minimising the difference between the random feature map approximation of the closure term $\psi(x) = \phi(x)$ over all grid points $x = X^{(k)}$, and the approximation of the closure term provided by the observations

$$\frac{X_n^{(k)} - X_{n-1}^{(k)}}{\Delta t} - G^{(k)}(\mathbf{X}_{n-1}).$$

This finite differencing, however, constitutes a bad estimator of the closure term $\psi(x)$ for noisy observations of the slow variables. In the following we therefore only present results for LR in the case of zero measurement error (i.e. the same setting in which the polynomial fits (40) and (41) were obtained). RAFDA, on the other hand, employs as

the forecast model within the data assimilation training phase the reduced model (39) where $\psi(x)$ is estimated using random feature maps $\psi(x) = \mathbf{W} \tanh(\mathbf{W}_{\text{in}}x + \mathbf{b}_{\text{in}})$ (cf. (6) and (7)). RAFDA is trained on $N = 100,000$ noisy observations of all components $X^{(k)}$ of \mathbf{X} with variance $\eta = 0.02$ sampled at $\Delta t = 0.0005$, and an initial ensemble chosen according to (29) with $\gamma = 0.01$. The validation is performed by propagating the reduced model (39) with the learned mapping $\psi(x)$ added at each grid point in an Euler time-stepping method with step-size $\delta t = 0.005$ for a total of 10^6 time steps.

Figure 11 shows the closure term $\psi(x)$ estimated from RAFDA, LR and from the polynomial fits (40)–(41). We show in Figure 12 the empirical probability density function of the validation time series and list in Table 1 the associated relative errors of the mean and the variance of \mathbf{X} for the various parametrization schemes used. The closure model provided by RAFDA outperforms both the closure of LR and the one given by (40)–(41). It is seen that the reference empirical probability density function of the full multi-scale L96 system assigns more probability to higher values of \mathbf{X} . We conjecture that this underdispersiveness of the closure models stems from their assumed deterministic nature. The deterministic closures schemes considered here ignore the effective diffusive effect of the fast variables which are present for finite time-scale and spatial-scale separation. As a first step towards a full stochastic parametrization one could use RAFDA to learn the propagator of the mean $E^{(k)} = \sum_{j=1}^J Y^{(j,k)}$ alongside the mapping $\psi(x)$.

TABLE 1. Relative error of the mean μ and the variance σ^2 of the slow variables \mathbf{X} for the various parametrization schemes.

	μ	σ^2
RAFDA	0.0056	0.019
LR	0.029	0.028
Wilks	0.033	0.065
Arnold et al.	0.016	0.063

6. DISCUSSION AND OUTLOOK

We have proposed a new data-driven physics-agnostic forecast model coined RAFDA which combines random feature maps with DA. The method is designed to provide cheap surrogate mappings to be used in forecasting or to construct closure models when no *a priori* knowledge of the evolution equations is available and the underlying system is only accessible via noisy observations. The linear coefficients of the random feature map are sequentially updated incorporating incoming observations using an EnKF, which itself uses the random feature map as its forecast model. We have tested the forecast capabilities in several situations for ordinary and partial differential equations. For the Lorenz-63 model we were able to achieve a forecast horizon of up to 4 Lyapunov times, similarly for the Kuramoto-Sivashinsky equation. We investigated the influence on the data length, the number of feature maps and the

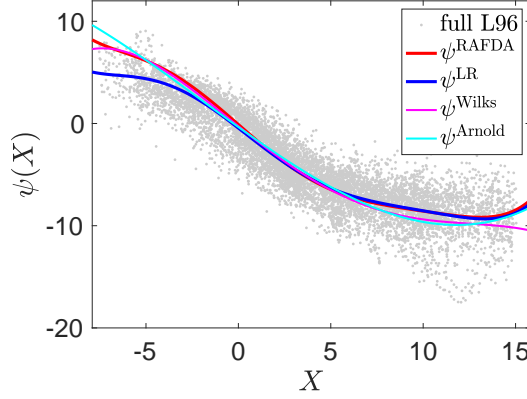


FIGURE 11. Closure terms $\psi = \psi(x)$ for the multi-scale L96-system (37)-(38) estimated using various parametrizations.

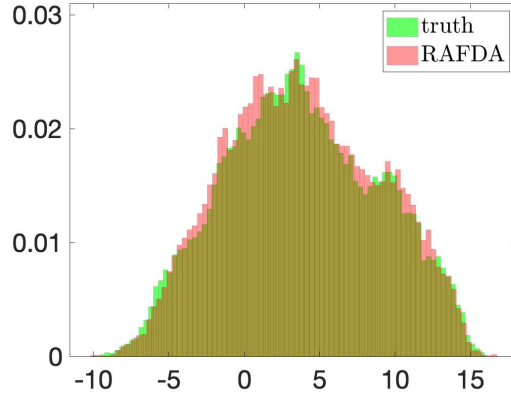


FIGURE 12. Empirical probability density function of the slow variables X_k of the full multi-scale L96-system (37)-(38) and of the RAFDA closure model.

noise strength on the forecast horizon. Depending on the dimension of the underlying dynamical system a larger number of random feature maps and larger training data sets are required. Once trained, however, the computational cost to run the model can be significantly cheaper than numerical integration of the original full model. For example, for the Kuramoto-Sivashinsky model we used a discretization time step of $\delta t = 10^{-3}$ whereas the surrogate RAFAD model was trained on a time series with $\Delta t = 0.25$, which implies a computational gain in running time of $\Delta t / \delta t = 250$. However, we stress that the real advantage of RAFDA becomes apparent when the model is unknown. Besides providing remarkable forecast skills for individual trajectories, we showed that ensembles generated by in data assimilation cycles which use a pre-trained RAFDA forecast model are reliable which makes them attractive

candidates for probabilistic forecasting where one would like to issue an uncertainty quantification of a forecast. Furthermore, we showed that the multi-scale Lorenz-96 model RAFDA allowed us to find a Markovian closure model for the resolved variables having only observed its slow variables. We note that the EnKF in augmented state space could be replaced by other data assimilation schemes such as proposed, for example, in Chen and Majda (2019).

An open question is how to choose the random parameters of the feature map. The universal approximation property ensures that any continuous function can be well approximated by a linear combination of the features, but it does not tell you how to choose the parameters and how many features are needed. We have shown that the forecasts capabilities sensitively depends on the random parameters and that parameters which lead to good approximation in the noiseless case may fail to approximate the forecast map when trained on noisy data. A natural extension is to determine the optimal parameters \mathbf{W}_{in} and \mathbf{b}_{in} simultaneously with \mathbf{W} , possibly using again an ensemble Kalman filter. Rather than random features which are related to RKHS the machine-learning framework would then consist of a two-layer network, and the corresponding spaces are Barron spaces (Chizat and Bach, 2018; Mei et al., 2018; Rotskoff and Vanden-Eijnden, 2018; Sirignano and Spiliopoulos, 2020; E et al., 2019). This extension is planned for further research.

ACKNOWLEDGMENTS

The work of SR has been partially funded by Deutsche Forschungsgemeinschaft (DFG, German Science Foundation) - SFB 1294/1 - 318763901.

REFERENCES

- J. L. Anderson and S. L. Anderson. A Monte Carlo implementation of the nonlinear filtering problem to produce ensemble assimilations and forecasts. *Monthly Weather Review*, 127(12):2741–2758, 1999. doi:10.1175/1520-0493(1999)127<2741:AMCIOT>2.0.CO;2.
- H. M. Arnold, I. M. Moroz, and T. N. Palmer. Stochastic parametrizations and model uncertainty in the Lorenz 96 system. *Philosophical Transactions of the Royal Society A: Mathematical, Physical and Engineering Sciences*, 371(1991):20110479, 2013. doi:10.1098/rsta.2011.0479.
- A. Atencia and I. Zawadzki. Analogs on the Lorenz attractor and ensemble spread. *Monthly Weather Review*, 145(4):1381–1400, 2017. doi:10.1175/MWR-D-16-0123.1.
- F. Bach. Breaking the curse of dimensionality with convex neural networks. *J. Mach. Learn. Research*, 18(19):1–53, 2017a. URL <http://jmlr.org/papers/v18/14-546.html>.
- F. Bach. On the equivalence between kernel quadrature rules and random feature expansions. *J. Mach. Learn. Research*, 18(21):1–38, 2017b. URL <http://www.jmlr.org/papers/v18/15-178.html>.

- A. Barron. Universal approximation bounds for superposition of a sigmoidal function. *IEEE Trans. on Inform. Theory*, 39:930–945, 1993. doi:10.1109/18.256500.
- R. Buizza, P. L. Houtekamer, G. Pellerin, Z. Toth, Y. Zhu, and M. Wei. A comparison of the ECMWF, MSC, and NCEP global ensemble prediction systems. *Monthly Weather Review*, 133(5):1076–1097, 2005. doi:10.1175/MWR2905.1.
- G. Burgers, P. J. van Leeuwen, and G. Evensen. Analysis scheme in the ensemble Kalman filter. *Monthly Weather Review*, 126(6):1719–1724, 1998. doi:10.1175/1520-0493(1998)126<1719:ASITEK>2.0.CO;2.
- N. Chen and A. J. Majda. A new efficient parameter estimation algorithm for high-dimensional complex nonlinear turbulent dynamical systems with partial observations. *Journal of Computational Physics*, 397:108836, 2019. doi:10.1016/j.jcp.2019.07.035.
- L. Chizat and F. Bach. On the global convergence of gradient descent for over-parameterized models using optimal transport. *Advances in neural information processing systems*,, pages 3036–3046, 2018.
- G. Cybenko. Approximation by superposition of a sigmoidal function. *Math. Contr., Sign., and Syst.*, 2:303–314, 1989. doi:10.1007/BF02551274.
- W. E, C. Ma, and L. Wu. A priori estimates of the population risk for two-layer neural networks. *Commun. Math. Sci.*, 17(5):1407–1425, 2019. doi:10.4310/CMS.2019.v17.n5.a11.
- R. Edson, J. Bunder, T. Mattner, and A. Roberts. Lyapunov exponents of the Kuramoto–Sivashinsky PDE. *ANZIAM Journal*, 61(0):270–285, 2019. doi:10.21914/anziamj.v61i0.13939.
- E. S. Epstein. Stochastic dynamic prediction. *Tellus*, 21(6):739–759, 1969. doi:10.1111/j.2153-3490.1969.tb00483.x.
- G. Evensen. *Data Assimilation: The Ensemble Kalman Filter*. Springer, New York, 2006.
- B. Giggins and G. A. Gottwald. Stochastically perturbed bred vectors in multi-scale systems. *Quarterly Journal of the Royal Meteorological Society*, 145:642–658, 2019. doi:10.1002/qj.3457.
- T. M. Hamill, J. S. Whitaker, and C. Snyder. Distance-dependent filtering of background covariance estimates in an ensemble Kalman filter. *Monthly Weather Review*, 129(11):2776–2790, 2001. doi:10.1175/1520-0493(2001)129<2776:DDFOBE>2.0.CO;2.
- F. Hamilton, T. Berry, and T. Sauer. Ensemble kalman filtering without a model. *Phys. Rev. X*, 6:011021, Mar 2016. doi:10.1103/PhysRevX.6.011021.
- S. Herrera, J. Fernández, M. Rodríguez, and J. Gutiérrez. Spatio-temporal error growth in the multi-scale Lorenz-96 model. *Nonlinear Processes in Geophysics*, 17(4):329, 2010. doi:10.5194/npg-17-329-2010.
- H. Hersbach. Decomposition of the continuous ranked probability score for ensemble prediction systems. *Weather and Forecasting*, 15(5):559–570, 2000. doi:10.1175/1520-0434(2000)015<0559:DOTCRP>2.0.CO;2.

- P. L. Houtekamer and H. L. Mitchell. Data assimilation using an ensemble Kalman filter technique. *Monthly Weather Review*, 126(3):796–811, 1998. doi:10.1175/1520-0493(1998)126<0796:DAUAEK>2.0.CO;2.
- P. L. Houtekamer and H. L. Mitchell. A sequential ensemble Kalman filter for atmospheric data assimilation. *Monthly Weather Review*, 129(1):123–136, 2001. doi:10.1175/1520-0493(2001)129<0123:ASEKFF>2.0.CO;2.
- P. L. Houtekamer and F. Zhang. Review of the ensemble Kalman filter for atmospheric data assimilation. *Monthly Weather Review*, 144(12):4489–4532, 2016. doi:10.1175/MWR-D-15-0440.1.
- H. Jaeger. A tutorial on training recurrent neural networks, covering BPPT, RTRL, EKF and the "echo state network" approach, 2002.
- H. Jaeger and H. Haas. Harnessing nonlinearity: Predicting chaotic systems and saving energy in wireless communication. *Science*, 304(5667):78–80, 2004. doi:10.1126/science.1091277.
- Y. Kuramoto and T. Tsuzuki. On the Formation of Dissipative structures in reaction-diffusion systems: Reductive perturbation approach. *Progress of Theoretical Physics*, 54(3):687–699, 09 1975. ISSN 0033-068X. doi:10.1143/PTP.54.687.
- Y. Kuramoto and T. Tsuzuki. Persistent propagation of concentration waves in dissipative media far from thermal equilibrium. *Progress of Theoretical Physics*, 55(2):356–369, 02 1976. ISSN 0033-068X. doi:10.1143/PTP.55.356.
- K. Law, A. Stuart, and K. Zygalakis. *Data assimilation: A mathematical introduction*. Springer-Verlag, New York, 2015.
- C. E. Leith. Theoretical skill of Monte Carlo forecasts. *Monthly Weather Review*, 102(6):409–418, 1974. doi:10.1175/1520-0493(1974)102<0409:TSOMCF>2.0.CO;2.
- M. Leutbecher and T. Palmer. Ensemble forecasting. *Journal of Computational Physics*, 227(7):3515 – 3539, 2008. ISSN 0021-9991. doi:10.1016/j.jcp.2007.02.014.
- E. N. Lorenz. Deterministic nonperiodic flow. *Journal of the Atmospheric Sciences*, 20(2):130–141, 1963. doi:10.1175/1520-0469(1963)020<0130:DNF>2.0.CO;2.
- E. N. Lorenz. A study of the predictability of a 28-variable atmospheric model. *Tellus*, 17(3):321–333, 1965. doi:10.3402/tellusa.v17i3.9076.
- E. N. Lorenz. Predictability: A problem partly solved. In T. Palmer, editor, *Proc. Seminar on predictability Vol. 1*, pages 1–18, Reading, UK, 1996. ECMWF.
- W. Maass, T. Natschläger, and H. Markram. Real-time computing without stable states: A new framework for neural computation based on perturbations. *Neural Computation*, 14(11):2531–2560, 2002. doi:10.1162/089976602760407955.
- A. Majda and J. Harlim. *Filtering Complex Turbulent Systems*. Cambridge University Press, Cambridge, 2012.
- S. Mei, A. Montanari, and P.-M. Nguyen. A mean field view of the landscape of two-layer neural networks. *Proc. Natl. Acad. Sci. USA*, 115(33):E7665–E7671, 2018. doi:10.1073/pnas.1806579115.
- N. Nelson and A. Stuart. The random feature model for input-output maps between Banach spaces, 2020. URL <https://arxiv.org/pdf/2005.10224>.

- T. N. Palmer. Extended-range atmospheric prediction and the Lorenz model. *Bulletin of the American Meteorological Society*, 74(1):49–66, 1993. doi:10.1175/1520-0477(1993)074<0049:ERAPAT>2.0.CO;2.
- J. Park and I. Sandberg. Universal approximation using radial-basis-function networks. *Neural Computation*, 3:246–257, 1991. doi:10.1162/neco.1991.3.2.246.
- J. Pathak, B. Hunt, M. Girvan, Z. Lu, and E. Ott. Model-free prediction of large spatiotemporally chaotic systems from data: A reservoir computing approach. *Phys. Rev. Lett.*, 120:024102, Jan 2018. doi:10.1103/PhysRevLett.120.024102.
- D. Qi and A. J. Majda. Using machine learning to predict extreme events in complex systems. *Proceedings of the National Academy of Sciences*, 117:52–59, 2020. doi:10.1073/pnas.1917285117.
- A. Rahimi and B. Recht. Random features for large-scale kernel machines. In J. C. Platt, D. Koller, Y. Singer, and S. T. Roweis, editors, *Advances in Neural Information Processing Systems 20*, pages 1177–1184. Curran Associates, Inc., 2008. URL <http://papers.nips.cc/paper/3182-random-features-for-large-scale-kernel-machines.pdf>.
- A. Rahimi and B. Recht. Uniform approximation of functions with random bases. In *2008 46th Annual Allerton Conference on Communication, Control, and Computing*, pages 555–561, 2008.
- S. Reich and C. Cotter. *Probabilistic forecasting and Bayesian data assimilation*. Cambridge University Press, New York, 2015.
- G. M. Rotskoff and E. Vanden-Eijnden. Neural networks as interacting particle systems: Asymptotic convexity of the loss landscape and universal scaling of the approximation error, 2018. URL <https://arXiv.org/pdf/1805.00915>.
- J. Sirignano and K. Spiliopoulos. Mean Field Analysis of Neural Networks: A Law of Large Numbers. *SIAM J. Appl. Math.*, 80(2):725–752, 2020. ISSN 0036-1399. doi:10.1137/18M1192184.
- G. Sivashinsky. Nonlinear analysis of hydrodynamic instability in laminar flames - I: Derivation of basic equations. *Acta Astronautica*, 4(11):1177 – 1206, 1977. ISSN 0094-5765. doi:10.1016/0094-5765(77)90096-0.
- G. I. Sivashinsky and D. M. Michelson. On irregular wavy flow of a liquid film down a vertical plane. *Progress of Theoretical Physics*, 63(6):2112–2114, 06 1980. ISSN 0033-068X. doi:10.1143/PTP.63.2112.
- Y. Sun, A. Gilbert, and A. Tewari. On the approximation capabilities of ReLU neural networks and random ReLU features, 2019. URL <https://arxiv.org/pdf/1801.04374>.
- R. Temam. *Infinite-dimensional dynamical systems in mechanics and physics*, volume 68 of *Applied Mathematical Sciences*. Springer-Verlag, New York, second edition, 1997. doi:10.1007/978-1-4612-0645-3.
- Z. Toth and E. Kalnay. Ensemble forecasting at NMC: The generation of perturbations. *Bulletin of the American Meteorological Society*, 74(12):2317–2330, 1993. doi:10.1175/1520-0477(1993)074<2317:EFANTG>2.0.CO;2.
- Z. Toth and E. Kalnay. Ensemble forecasting at NCEP and the breeding method. *Monthly Weather Review*, 125(12):3297–3319, 1997.

- doi:10.1175/1520-0493(1997)125<3297:EFANAT>2.0.CO;2.
- X. Wang and C. H. Bishop. A comparison of breeding and ensemble transform Kalman filter ensemble forecast schemes. *Journal of the Atmospheric Sciences*, 60(9):1140–1158, 2003. doi:10.1175/1520-0469(2003)060<1140:ACOBAE>2.0.CO;2.
- D. S. Wilks. Effects of stochastic parametrizations in the Lorenz '96 system. *Quarterly Journal of the Royal Meteorological Society*, 131(606):389–407, 2005. doi:10.1256/qj.04.03.
- D. S. Wilks. *Statistical Methods in the Atmospheric Sciences*. Elsevier, Oxford, 2006.